ADVANCED MATERIALS
www.advmat.de

# Robust and Versatile Biodegradable Unclonable Anti-Counterfeiting Labels with Multi-Mode Optical Encoding Using Protein-Mediated Luminescent Calcite Signatures

*Ziting Wang, Meng Li, Yinghao Fu, Yu Wang,* and Yanqing Lu**

**Physical unclonable functions (PUFs) are emerging as a cutting-edge technology for enhancing information security by providing robust security authentication and non-reproducible cryptographic keys. Incorporating renewable and biocompatible materials into PUFs ensures safety for handling, compatibility with biological systems, and reduced environmental impact. However, existing PUF platforms struggle to balance high encoding capacity, diversified encryption signatures, and versatile functionalities with sustainability and biocompatibility. Here, all-biomaterial-based unclonable anti-counterfeiting labels featuring multi-mode encoding, multi-level cryptographic keys, and multiple authentication operations are developed by imprinting biomimetic-grown calcites on versatile silk protein films. In this label, the inherent non-clonability comes from the randomized characteristics of calcites, mediated by silk protein during crystal growth. The successful embedding of photoluminescent molecules into calcite lattices, assisted by silk protein, allows the resulting platform to utilize fluorescence patterns alongside birefringence for high-capacity encoding. This design facilitates easy and rapid authentication through Hamming distance and convolutional neural networks using standard cameras and portable microscopes. Moreover, angle-dependent polarization patterns enable multi-level key generation, while multi-spectral fluorescence signals offer multi-channel keys. The developed anti-counterfeiting labels combine biodegradability, green manufacture, easy authentication, high-level complexity, low cost, robustness, patternability, and versatility, offering a practical and high-security solution to combat counterfeiting across various applications.**

## 1. Introduction

The rise of the Internet of Things and advances in information technology have exacerbated the problem of counterfeiting, making it a growing global issue.[1] From luxury commodities, banknotes, electronics, and cultural and artistic items, to food, pharmaceutical, and agricultural products, fake and shoddy goods have infiltrated every aspect of our daily lives.[2] This pervasive issue can result in a range of severe consequences, which not only hurt the economy but also seriously negatively impact national security, human health, and intellectual property rights, among other facets of our society. Through the years, diverse anti-counterfeiting technologies, including holograms,[3] structural colors,[4] watermarks,[5] luminescent materials,[6] and radio-frequency identification tags,[7] have been developed to enhance information security and to mitigate the adverse impacts posed by counterfeit goods. Nevertheless, these systems remain susceptible to imitation or replication by sophisticated counterfeiters due to their reproducible physical features generated by deterministic fabrication and encoding processes. Therefore, there is an urgent

Z. Wang, Y. Fu, Y. Wang, Y. Lu
National Laboratory of Solid State Microstructures
Key Laboratory of Intelligent Optical Sensing and Manipulation
College of Engineering and Applied Sciences
and Collaborative Innovation Center of Advanced Microstructures
Nanjing University
Nanjing 210023, China
E-mail: yuwang87@nju.edu.cn; yqlu@nju.edu.cn

M. Li
Laboratory for Advanced Biopolymers
Department of Civil and Environmental Engineering
Massachusetts Institute of Technology
Cambridge, MA 02142, USA

The ORCID identification number(s) for the author(s) of this article can be found under https://doi.org/10.1002/adma.202409170

**DOI: 10.1002/adma.202409170**

 

need to develop robust, versatile, and unbreakable information anti-counterfeiting strategies to safeguard information from unauthorized access and replication.

PUFs have recently emerged as a cutting-edge technology to provide robust and unclonable security authentication.[8] A PUF takes advantage of the inherent randomness of a physical system introduced during the non-deterministic fabrication process to generate a stochastic, unique, and unpredictable output (response) under an external stimulus (challenge).[9] Since the identifier or key generated by a PUF is derived from the intrinsic random features of the physical system and is not assigned by an outside source, it is extremely difficult to copy or imitate, making the PUF a highly secure and hard-to-break approach to identification and encryption. Since the first proposal of the PUF concept by Pappu et al.,[8a] a diverse array of novel PUF technologies has emerged. Silicon PUFs relying on the intrinsic variability in the complementary metal-oxide semiconductor manufacturing process have experienced sustained success across various fields, including anti-counterfeiting and information encryption systems, identity authentication and authorization, etc.[10] Although these integrated-circuits-based PUFs show the merits of high throughput and ease of integration into existing semiconductor manufacturing workflows, they suffer from limited bit stability, low entropy, and vulnerability to physical attacks. More recently, non-silicon PUFs as security labels that depend on materials with distinct physicochemical properties have become increasingly popular owing to their advantages of flexibility, huge coding capacity, high output complexity, and resistance to software-based attacks.[9] These systems can be based on various physical phenomena, such as the randomness of optical properties,[11] the variability of magnetic materials,[12] or the uniqueness of biological structures.[13]

As a representative type of non-silicon PUFs, optical PUFs have gained significant attention because of the non-contact and rapid optical readout and the diversity in regulating the optical properties with multiple degrees of freedom (amplitude, phase, wavelength, polarization, lifetime, etc.). In recent years, significant advancements have been made in creating optical PUFs based on photoluminescence,[14] structural color,[15] hologram,[16] polarization,[17] Raman spectra,[11a,18] and scattering signals.[19] A wide range of materials were studied such as carbon dots,[20] quantum dots,[21] diamond microparticles,[11b,22] liquid crystals,[23] silk proteins,[2e,24] DNA,[25] and salt solution.[26] The development of the new generation of optical PUFs has opened doors for an extensive array of applications, including identification marks for IDs, and anti-counterfeiting labels for commodities that enable a seamless security platform from production, logistics, and sales, all the way to usage. Despite the prominent advances toward high-security anti-counterfeiting, most existing optical PUF comprising non-renewable, non-biocompatible, and non-biodegradable components can pose environmental risks and health hazards when used to manufacture products that come into direct contact with biological systems either during usage or after improper disposal. This issue can be effectively overcome using naturally derived biomaterials.[2e,24,25,27] However, existing PUF platforms derived from biological materials feature only simple encrypted signatures and thus offer a limited authentication approach, reducing the PUF system's complexity, hence increasing the risk of being hacked. Meanwhile, most biological-material-based PUF platforms rely on intricate and energy-intensive manufacturing processes to generate the random physical signal and use bulky setups to authenticate. Accordingly, a novel strategy is required to integrate sustainable material sourcing, inherent randomness, simple fabrication, and robust security encryption with authentication facilitation within a single PUF platform to effectively address the diverse needs of multiple applications.

Calcium carbonate ($CaCO_3$), one of the most ubiquitous minerals in nature, can be abundantly found in various biological organisms like the skeletons of corals and sea urchins, the shells of mollusks, and the eggshells of vertebrates.[28] During the biomineralization formation of these biological materials, biological organic matrices are involved to control and direct the crystallization of calcium carbonate.[29] This strategy has motivated the application of biomimetic mineralization techniques to synthesize artificial calcium carbonate biominerals that exhibit diverse crystal types, textures, morphologies, and physical properties. Among the various crystalline forms of calcium carbonate, calcite is one of the most prevalent forms, owing to its excellent optical birefringence, exceptional chemical and thermal stability, and robust mechanical properties.[30] Through the mediation of organic matrices, calcite crystals with unique surface textures, morphologies, and geometrical dimensions—and consequently unique optical characteristics—can be easily obtained and modulated by adjusting their mineralization conditions.[31] By selecting an appropriate mineralization method, one can grow a layer of randomly distributed calcite crystals on the surface of a solid substrate.[32] Consequently, this inherent uniqueness and randomness prevent accurate replication or forgery, making these crystals with specific optical responses potential for developing optical PUF labels. Additionally, the capacity to introduce optical functional components into the growth process of calcite under the mediation of organic matrices[33] further enhances its optical functionalities, thereby adding complexity to encoding and anti-counterfeiting. Thus, the multiple degrees of freedom offered by calcite biomimetic mineralization growth present an excellent opportunity for constructing advanced PUFs with high-security features. However, the application of biomimetic mineralized calcites in optical anti-counterfeiting and PUF labeling has not been previously documented.

Here, we report the construction of calcite-based biodegradable, reliable, and robust PUF labels that integrate multi-mode optical encoding, multi-level cryptographic keys, and multiple authentication methods in a single platform, by leveraging a combination of biomimetic mineralization and multi-strategy imprinting techniques. The developed calcite PUFs, composed entirely of sustainable and biocompatible materials, represent breakthroughs in encoding diversity, eco-friendly manufacturing, authentication ease, stability, high capacity, and versatility compared to existing PUF labels derived from biological sources (Table S1, Supporting Information). The birefringence pattern and photo-luminescence signal are utilized to enable multi-mode optical encoding, which can be authenticated using Hamming distance (HD) and convolutional neural network algorithms. Moreover, the angular-dependent readout of the birefringence pattern and wavelength-dependent readout of the photo-luminescence signal are further explored to achieve multi-level and multi-channel high-security cryptographic keys.

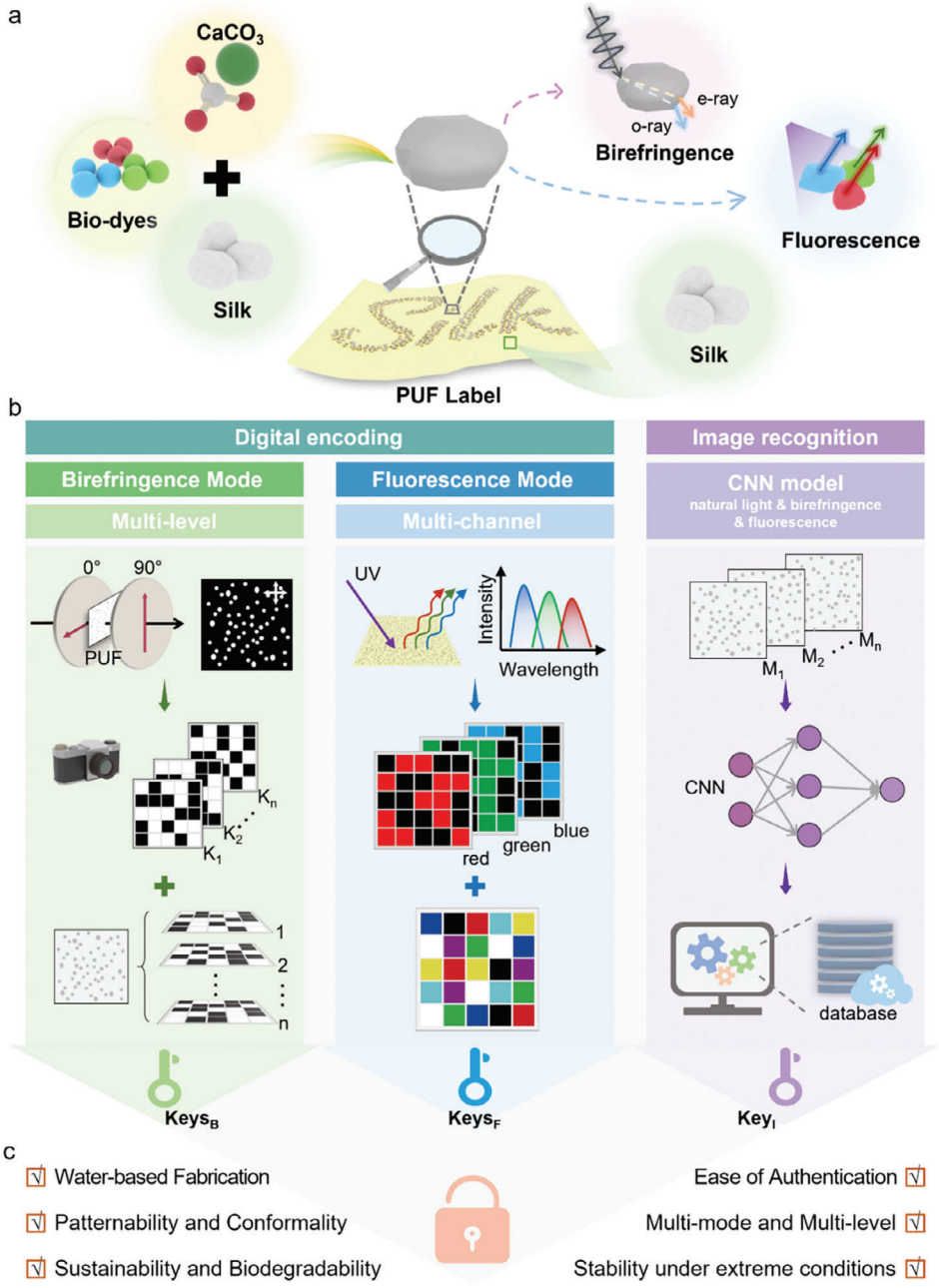


**Figure 1.** Anti-counterfeiting labels based on fluorescent calcites on biodegradable silk protein substrate. a) Schematic of the all-biomaterial-based PUF label, showing the composition and optical responses of the fluorescent calcites imprinted on flexible silk film. b) Schematic illustration of the multiple authentication operations, multi-mode optical encoding, and multi-level cryptographic key generation. c) The advantageous characteristics of the developed calcite PUFs.

Furthermore, we show that the exploited calcite PUF labels exhibit exceptional robustness under extreme conditions, including high temperature (200 °C), mechanical stripping, UV light irradiation, and high humidity (70–80%), while being cost-effective and biodegradable in soil environments. Finally, we demonstrate that the attributes of patternability, co-conformal surface contact capability, and biodegradability enable calcite PUFs to serve as a reliable and effective approach for establishing unbreakable anti-counterfeiting measures.

## 2. Results and Discussion

### 2.1. Calcite PUF Labels with Encoding Diversity and Material Versatility

**Figure** 1a illustrates the structural assembly of the calcite PUF label, featuring a disordered array of patterned monolayer calcite microcrystals embedded within a silk protein film, achieved through the integration of biomimetic mineralization and

imprinting techniques. The materials used to fabricate the PUF label—silk fibroin, calcite, and bio-dye—are renewable and biocompatible, excluding the use of non-sustainable or toxic substances that could be harmful to the environment or incompatible with biological systems. The randomly arranged calcite crystal monolayer, obtained via the biomimetic mineralization growth, generates birefringent signals intrinsic to the crystals, along with fluorescent signals emitted by the introduced bio-dyes. In this process, the incorporation of silk protein plays a crucial role in determining the overall structural organization and optical functionality of the resulting calcites. On the one hand, the employment of silk protein as an organic mediator regulates the nucleation and growth of calcite crystals, resulting in crystals with varied morphologies, geometrical dimensions, surface textures, and distributions, which is essential for the successful application of calcite microcrystals in optical PUFs. On the other hand, the presence of silk proteins enables the successful embedding of fluorescent dyes into lattices of microscale calcite crystals during their growth, thereby imparting photoluminescence to the crystals. This biomimetic mineralization process enables the three material components to "grow" together, which is crucial for enhancing structural integrity and functional properties. On this basis, these grown monolayers of calcites can be facilely transferred to silk protein films by utilizing the water vapor-assisted imprinting ability of silk proteins as demonstrated in our previous study,[34] to create flexible, biodegradable, robust, and versatile non-cloneable anti-counterfeiting platforms.

For these calcite-based optical PUF labels, the unique birefringence properties and colors of each calcite crystal under orthogonally polarized light make them suitable for creating unique security patterns that can be used to verify the authenticity of the PUFs. Since calcite is a uniaxial crystal,[30a] the intensity of birefringence varies with the angle between the crystal's optical axis and the orthogonal polarizers. By leveraging this concept and the disordered distribution of optical axes, it becomes possible to construct multi-level physical unclonable codes (or keys). In the meantime, the incorporated fluorescent elements offer a luminescent anti-counterfeiting feature, thereby providing another effective, crosstalk-free means for PUF authentication. For color-based optical response, we can integrate fluorescent calcite with different emission bands onto the same silk protein substrate through multi-step imprinting processes, thus endowing the PUFs with multi-channel encoding capability. Overall, the developed PUF labels can exhibit two distinct forms of challenge-response pairs (CRPs) in the birefringence and fluorescence modes. Combined with the feature that even within a single mode one can generate multiple cryptographic keys, these PUF labels can lead to a multi-mode and multi-level anti-counterfeiting authentication system. Notably, compared to existing optical PUF platforms based on birefringence and fluorescence,[2e,14a,23a,24a] the dense and rigid nature of calcite crystals significantly enhances the robustness of its birefringence and the stability of embedded fluorescent dyes. This ensures that PUF labels maintain strong birefringent and fluorescent signals under varying environmental conditions and during prolonged usage (see details below), making calcite-based PUF labels highly promising for practical applications.

Figure 1b summarizes the multi-mode encoding process, multi-level cryptographic key generation, and multiple authentication methods of the calcite-PUF labels. The birefringence mode is credited to the crystalline structures of the calcites, the signal can be read out by polarized light. The birefringence mode comprises two forms: a one-step certification process using only a macro-lens-equipped digital camera, and a multi-level certification approach enabled by the aforementioned angular-dependent readout. The fluorescence mode stems from the incorporated fluorescent dyes, it can be read out by UV light. The fluorescence mode also comprises two forms: three independent channels for the RGB colors and a combined mode that mixes the RGB channels for an 8-valued coding. These CRPs can be used to generate multiple unpredictable digitized keys, enabling independent encryption functions across two modes. In addition to digital encoding, when combined with deep learning technology, the image recognition function can be realized to generate an additional digital key. Users have the flexibility to choose one authentication method or combine them to meet their needs regarding the security level and accessibility to readout equipment.

The PUF labels can be read using a macro-lens-equipped camera and a portable microscope, eliminating the need for bulky optical devices or specialized operator skills. Meanwhile, the combination of silk fibroin substrate and imprinting technology makes the PUF label flexible, patternable, and conformal to meet users' personalized labeling needs. Last but not least, this PUF label is sustainable, and biodegradable and exhibits thermal, mechanical, UV, and chemical stability, ensuring its reliability under various conditions. These favorable characteristics of the developed calcite PUFs are generalized in Figure 1c.

### 2.2. Fabrication of the Calcite PUF Labels

The fabrication process of PUF labels involves two main steps (shown in **Figure 2a**)— growing luminescent calcite crystals on a glass substrate and imprinting these crystals onto a silk substrate. First, we grew calcite-type calcium carbonate microparticles using a silk protein-mediated mineralization approach, following the previously described method.[35] The 1% w/v silk fibroin solution was mixed with an equivalent mass of 20 mmol $L^{-1}$ $CaCl_2$ solution and the mixture was poured into three beakers. To produce fluorescently labeled calcite crystals, three different fluorescent dyes—blue, green, and red—were separately added to individual beakers and mixed thoroughly. (Figure 2a-i). Subsequently, a clean cover glass was suspended at the liquid-air interface in each beaker. All the beakers were sealed with perforated parafilm and placed into a desiccator (Figure 2a-ii) along with $(NH_4)_2CO_3$ powders. After resting for 48 hours at room temperature, three different fluorescent-colored calcites—blue fluorescent calcites (B-calcites), green fluorescent calcites (G-calcites), and orange-red fluorescent calcites (O-calcites) were individually obtained on the side of the cover glass in contact with the liquid (Figure 2a-iii). The addition of silk proteins mediates nucleation sites, growth mechanisms, morphologies, and surface textures of $CaCO_3$ crystals, thus influencing the final characteristics of the crystals.[35,36] Specifically, the presence of silk protein chains in the solution "gently" inhibits the nucleation process of $CaCO_3$ in the solution, therefore favoring nucleation at the liquid-substrate interface.[32b,35] Meanwhile, silk protein restrains the reaction dynamics, favoring the transition toward

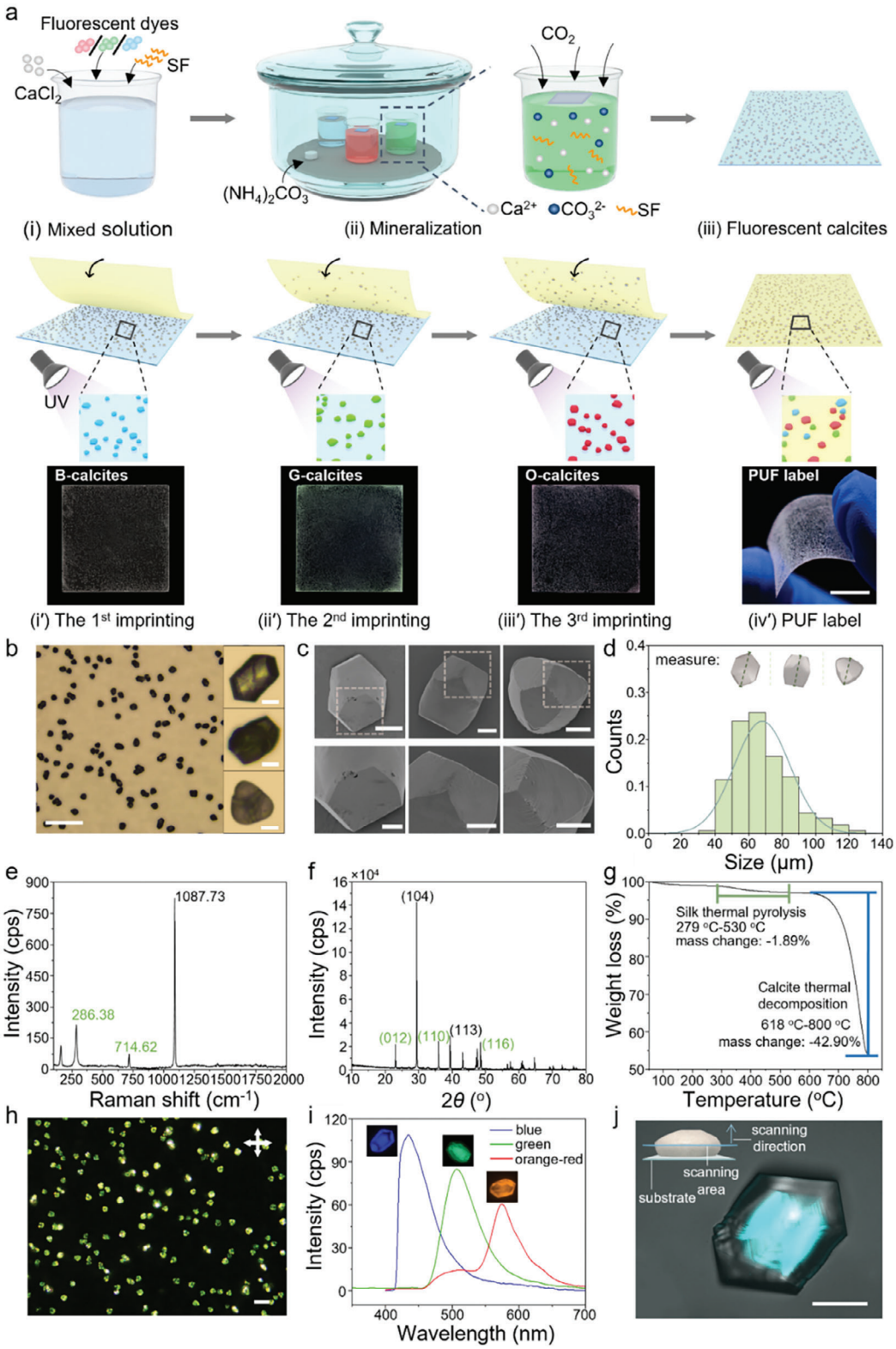


**Figure 2.** Fabrication and characterization of the PUF label. a) Schematic illustration of the fabrication process of the PUF label. i-iii) Formation of fluorescent calcites on a glass substrate. i) Mixed silk fibroin, fluorescent dyes, and $CaCl_2$ solution in a beaker. ii) Mineralization process. iii) Randomly distributed fluorescent calcites on a glass substrate. i′-iv′) (Top) Formation of the PUF label. i′-iii′) Step-by-step imprinting transfer of blue (i′), green (ii′), and red (iii′) colored fluorescent calcites. iv′) The obtained PUF label with three different fluorescent color calcites. (Bottom) Corresponding photographs taken with normal light illumination showing the randomly grown calcite microparticles and the final PUF label. Scale bar: 1 cm. b) The

thermal equilibrium.[37] During the growth process, silk fibroin effectively regulates the morphology of $CaCO_3$ and, due to its inherently disordered molecular structure, demonstrates diverse regulatory capabilities. Furthermore, the silk protein exhibits a directed adsorption effect on the crystal faces, which in turn results in the modification of specific crystalline surfaces of calcite.[38] As a result, the mineralization process regulated by the silk protein molecules ultimately leads to the forming of a layer of thermodynamic equilibrium product—calcite microparticles with varied morphologies and modified crystal faces—on the glass substrate.

Based on this, flexible PUF labels were then prepared by fusing three different colored-fluorescent calcites onto a silk film through water-vapor-assisted step-by-step imprinting transfer (Figure 2a i′-iv′, top). The imprinting transfer method used here exploits water-vapor-induced molecular chain softening and rearrangement of amorphous silk proteins, as detailed in our previous study.[34] The inherent randomness of the calcites was preserved during the imprinting steps (Figure 2a i′-iv′, bottom). The fabrication process described above is all-water-based and accessible without using complex large-scale equipment or stringent vacuum conditions, which are crucial for scaling up production for widespread adoption. Moreover, by carefully controlling the temperature and exposure time of water vapor, the thorough "melting" of silk protein in the regions directly exposed to water vapor ensures robust adhesion of calcite particles to the silk substrate, which enhances the overall stability of the PUF label. Furthermore, the spatially controllable nature of the imprinting transfer technique employed here enables the construction of patterned calcite arrays on a silk substrate (Figure S1, Supporting Information) to further enhance the functionality and customization of the PUF platforms.

### 2.3. Characterization of the Calcites Microparticles

The introduction of silk protein and fluorescent molecules during $CaCO_3$ crystal growth provides a high degree of control over the specific morphologies and optical properties of crystals. The optical microscope images and scanning electron microscope (SEM) images (Figure 2b,c) display the randomness in the size, shape, and distribution of calcites on the glass substrate. The crystals have a wide size distribution with a mean value of ≈60 µm (Figure 2d). The sizes and number of calcites can be tuned by adjusting the mineralization parameters such as growth time and $CO_2$ concentration (see Figures S2 and S3, Supporting Information for details). Furthermore, influenced by the regulation of silk protein chains, the calcites primarily display three distinct crystal shapes (inset images in Figure 2b) with excellent randomness in spatial distribution, a significant difference from the calcite crystals formed without the addition of silk protein (Figure S4, Supporting Information). More specifically, the selective adsorption of silk proteins onto the crystal surfaces results in varying morphologies among different surfaces of the same crystal (Figure 2c), further augmenting the entropy of the system. This tunable size and number, combined with the randomness of crystal shape and surface morphology, enhances the uniqueness and unpredictability of the PUF labels, making them highly secure and virtually impossible to replicate or counterfeit.

The polymorph of the grown crystals was examined using Raman spectroscopy (Figure 2e) and X-ray powder diffraction (XRD) (Figure 2f). Both results confirm the exclusive presence of the calcite polymorph.[39] Thermogravimetric analysis (TGA) result confirms the presence of silk protein in the grown calcite crystals. As shown in Figure 2g, at temperatures below the thermal decomposition point of $CaCO_3$ crystals (600 to 800 °C), a weight loss of 1.89% occurs from 279 to 530 °C, with the maximum weight loss peak at 346 °C, which is attributed to the thermal pyrolysis of silk protein.[40]

While the addition of silk protein regulates the morphology of calcite crystals, the intrinsic birefringence properties of natural calcites still apply to the grown ones presented here. As shown in Figure 2h, the grown calcites display vivid birefringence colors under orthogonal polarizers. It is worth noting that the brightness of the birefringence color varies based on the angle formed between the orthogonal polarizers and the optical axis of the calcite particles (see below for details). At the same time, incorporating fluorescent molecules into the growth process of calcites endows them with bright fluorescent colors under ultraviolet light. As illustrated in Figure 2i, B-calcites, G-calcites, and O-calcites exhibit distinct fluorescence properties with non-overlapping emission peak positions. Under laser confocal microscopy, the stratified scan results reveal that the center of the calcite exhibits a higher fluorescence intensity than its surface areas (Figure 2j; Movie S1, Supporting Information). This result demonstrates that the fluorescent molecules are primarily incorporated during the early stages of crystal growth (Figure S5, Supporting Information). This unique fluorescence distribution enhances the stability of calcite's fluorescence property, resulting in a more stable fluorescence signal output. It is worth noting that the calcites with the addition of fluorescent dye but without the inclusion of silk protein during the mineralization process are essentially non-fluorescent (Figure S6, Supporting Information), indicating that fluorescent molecules can only be embedded into the crystals with the assistance of silk protein, as previously reported.[33]

### 2.4. The Digital Encoding of PUFs in the Birefringence Mode

The birefringence signals of the calcite microparticles can be harnessed as an effective authentication method for cryptographic

optical microscopy image of prepared randomly dispersed calcite particles. Scale bars: 250 µm. The inset images present three typical morphologies of grown calcites. Scale bars: 25 µm. c) The SEM images showing the unique surface texture of three typical calcites. Scale bars: 25 µm (top), 10 µm (bottom). d) The size distribution of calcites with the green line indicating the Gaussian fit. The inset images depict the measurement of the size of three distinct calcite microparticles. e,f) Raman (e) and XRD (f) spectra of the fluorescent calcites. The calcite's characteristic peaks are highlighted in green font. g) TGA curve showing the thermal decomposition of silk protein and $CaCO_3$. h) Polarized optical microscopy image showing the random orientation of the crystal axis of the grown calcites. Scale bar: 100 µm. i) The fluorescence intensity of B-calcites, G-calcites, and O-calcites, respectively. j) Laser confocal microscopy image under an excitation wavelength of 405 nm, indicating the generation of fluorescence within the calcite. The inset shows the layer-by-layer scanning process. Scale bar: 25 µm.

keys. Because of their distinctive birefringence properties and suitable size, these calcites can be visualized using a portable setup—a camera equipped with a macro lens and two polarizers (Figure S7, Supporting Information), providing PUF labels with convenient, cost-effective, and rapid readout capabilities. To generate a quantitative analysis of PUF readouts, we cut out 5 mm × 5 mm PUF samples from the larger imprinted silk film for subsequent experiments (**Figure 3**a,b). The image of this area was resized to 50 pixels × 50 pixels, converted to grayscale (Figure 3c), and then binarized to black-and-white images using the median of the sample birefringence intensity as the threshold (Figure 3d). These white and black pixels correspond to 1-bits and 0-bits respectively. The optical security keys of these PUF labels in birefringence mode rely on the unique combinations of 1-bits and 0-bits.

Generally, PUF labels can be evaluated based on three important indicators: bit uniformity, uniqueness, and repeatability, which collectively assess their security and quality (Details see Note S1, Supporting Information). Bit uniformity refers to the probability of the 1-bits and 0-bits appearing in the code, demanding a true random response to having a 50% probability of being 0 or 1 for each pixel. In this ideal case, the PUF labels' output response has the maximum number of random binary code combinations. We considered a 50 pixels × 50 pixels binarized image as a security key and calculated the average value of bit uniformity across 100 PUF labels. The result value is 0.4999 (Figure 3e), which is quite close to the ideal uniformity value of 0.5. This indicates that the PUF labels underlie the birefringence mode possess a high degree of randomness in pixel distribution, ensuring overall security.

Uniqueness or the average inter-HD (i.e., the variations between different PUFs under the same challenge) defines how well the response of one PUF distinguishes itself from the rest of the pool, ensuring that a PUF label is not duplicated and cannot be replaced. In an ideal PUF system, the responses between two different PUFs should exhibit completely uncorrelated bits, implying that the average inter-HD should be 0.5. In our PUF system, the uniqueness of 100 PUF labels under birefringence mode exhibits a mean value of 0.5001 (Figure 3f). These close-to-ideal-value results demonstrate the good uniqueness of our PUF labels in birefringence mode.

Repeatability or the average intra-HD (i.e., the differences between identical PUFs) quantifies the consistency of PUF readouts across multiple measurements. It is crucial for a PUF label to give the same readouts under the same challenge steadily. The ideal repeatability value is 0, indicating that codes obtained from the same PUF are repetitively identical. Among the 100 PUF labels we analyzed, the average intra-HD was calculated to assess the repeatability. As illustrated in Figure 3f (shown in green bars), the intra-HDs from the first and second measurements of the same PUF labels give an average value (repeatability) of 0.0234, which is near the ideal repeatability of 0 and show good repeatability in our PUF system. Furthermore, the diagonal data in Figure 3g is also close to zero, also indicating good repeatability of the PUF labels in birefringence mode.

Based on this encoding mode, we calculated the theoretical coding capacity of the PUF label. It refers to the maximum number of CRPs that the PUF label can generate, which is the basis of PUF security. The encoding capacity can be calculated using $C^n$, where $C$ represents the number of responses for each pixel (or bit level), and $n$ represents the number of pixels. In this birefringence mode, the value of $C$ is 2, corresponds to the binary outcome. We partitioned the image into 50 pixels × 50 pixels, resulting in an encoding capacity of $2^{2500}$ ($\approx 3.76 \times 10^{752}$), which is a good capacity size. Furthermore, the encoding capacity of the PUF label can be increased with the expansion of the bit level. When we performed the encoding matrix in quaternary, decimal, and hexadecimal (M-ary encoding) of the PUF label under birefringence mode with a resolution of 50 pixels × 50 pixels, its encoding capacity would be expanded to $4^{2500}$ ($\approx 1.41 \times 10^{1505}$), $10^{2500}$, and $16^{2500}$ ($\approx 2.0 \times 10^{3010}$), respectively (Figure S8, Supporting Information). In the case of M-ary encoding, the PUF label still maintains good performance. The uniqueness in quaternary, decimal, and hexadecimal are 0.7490, 0.8836, and 0.9147, respectively, which are very close to the ideal values of 0.75, 0.9, and 0.9375, respectively (Figure S8b, Supporting Information). However, it is worth noting that with the sharp increase in the code length, the subtle differences caused by the device or environmental disturbance during image capture can no longer be ignored. In this context, intra-HD is no longer suitable for representing the repeatability of PUF.[27c] Thus, we used the correlation coefficient (CC) to represent the repeatability of the two test results (Figure S8c,d, Supporting Information). After measuring the same PUF label twice, the absolute value of the CC of the results is very close to 1, indicating a strong correlation between the two measurements. In contrast, the CC for different PUF labels is close to 0. Notably, the encoding capability of the PUF labels can be further improved by optimizing the growth size and density of calcite crystals and thus increasing the number of encoded pixels. Specifically, given a certain calcite particle density, smaller particle sizes allow for more pixels to be divided per unit area, thereby increasing the encoding capacity of the PUF label. However, the particle size must remain within a range that is recognizable by the camera to meet the requirement for simple authentication. Conversely, with a fixed particle size, increasing the particle density allows for more pixels to be divided, thus improving the encoding capacity of the PUF. The particle density must also ensure a sufficiently random distribution, with bit uniformity close to the ideal value of 0.5 for binary encoding. If the density is too high, the encoding of the PUF may become biased toward 1 bit, which would reduce the overall performance of the PUF.

By further introducing angular variations in polarization, we can achieve multi-level PUF codes with more complex encoding and higher security. As shown in Figure 3h, with the polarizer and analyzer maintained in an orthogonal state, variations in the angle between the PUF label and the orthogonal polarizers result in changes in the birefringence intensity of the PUF labels. Each time when the optical axis of the calcite is parallel to the direction of either the polarizer or the analyzer, an extinction occurs with no birefringence signal. Hence, during a full rotation of the PUF label, the birefringence signal undergoes 4 cycles of periodic intensity change: extinction occurs every 90°, and peak values occur in between (Figures S9 and S10, Supporting Information). The observed angular-dependent birefringence intensity, akin to natural calcite, an optical uniaxial crystal, further validates that the grown calcites regulated by silk fibroin with embedded fluorescent dyes possess a similar birefringence behavior as natural ones (Figure S9, Supporting Information). Based on this

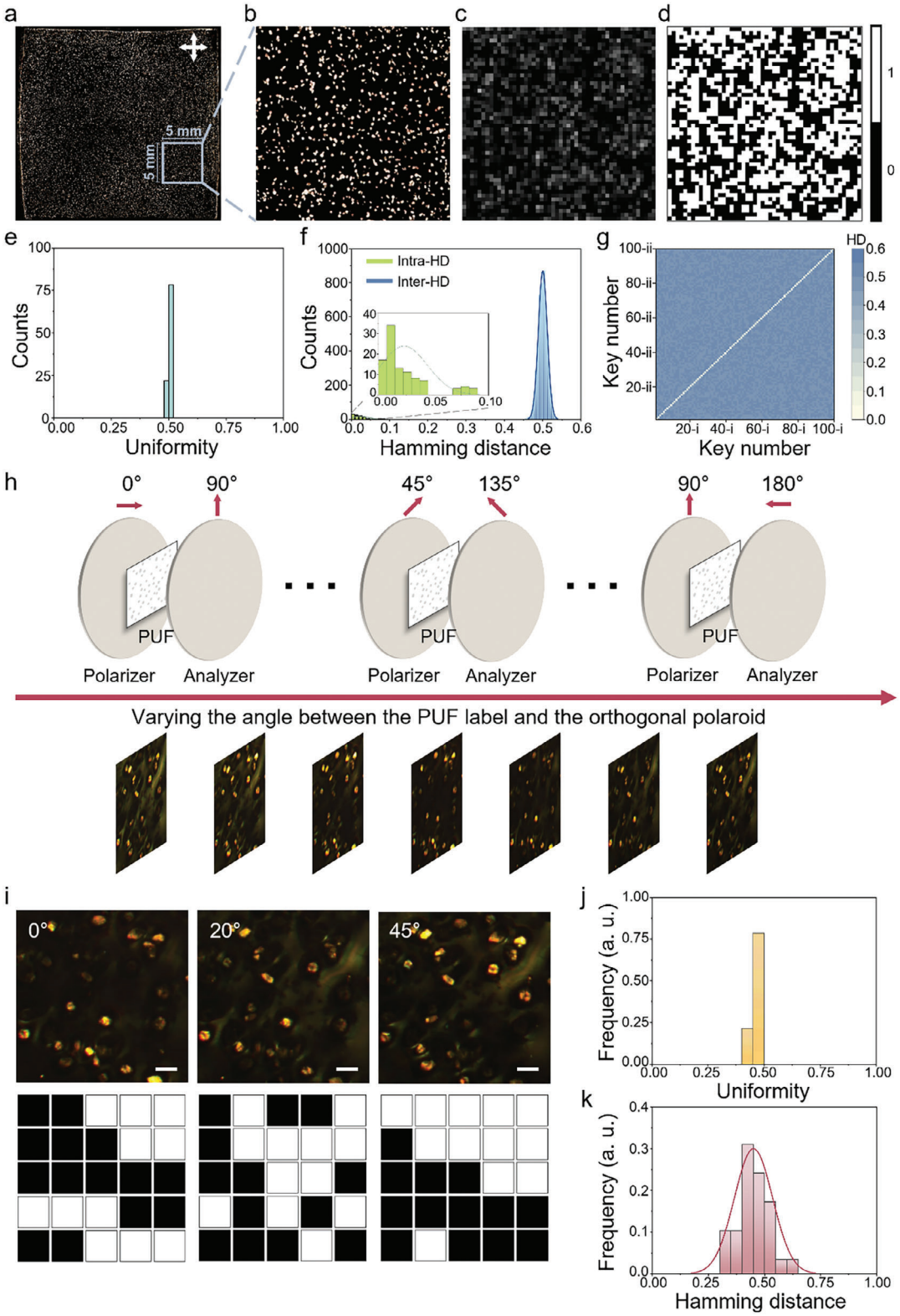


**Figure 3.** Encoding of PUF labels in the birefringence mode. a) Birefringence image of a calcite PUF label taken by a camera under orthogonal polarizers (size: 2.4 cm × 2.4 cm). b) Enlarged detail of the gray dashed area in (a) (size: 5 mm × 5 mm). c) Gray image corresponding to the birefringence image in (b). d) The corresponding 2D binary image encoding matrix of (c) based on dark (0) and bright (1) levels at each pixel (resolution: 50 pixels × 50 pixels). e) Bit uniformity of the 100 PUF labels. The average value is 0.4999. f) Inter-HD and intra-HD calculated among 100 PUF samples. The average inter-HD is 0.5001 with a standard deviation of 0.0116, while the average intra-HD is 0.0234 with a standard deviation of 0.0212. g) Pairwise comparison

angular-dependent birefringence signal and the random optical axis distribution of each calcite, we can encode information into the orientation of each calcite, thereby enabling angle-dependent encoding and authentication. Using multiple binary codes at different angles of the same PUF label, we enhance the entropy of the system by many folds. It will make replicating the PUF label even harder; besides the pixel distribution, the brightness variation based on calcite orientation would also have to match. We prepared 10 PUF labels and designated an initial angle to be 0 degrees. Subsequently, we captured images of each PUF label at 0 degrees, 20 degrees, and 45 degrees, respectively, and converted them into 5 pixels × 5 pixels binary format (Figure 3i). This process was repeated for each PUF label. We calculated the bit uniformity and uniqueness of the three-level binary codes obtained from the same PUF label at three different angles. The average bit uniformity is 0.4627 (Figure 3j) while the mean inter-HD of the binary codes is 0.4507 (Figure 3k). Since the optical axis orientation and the maximum birefringence intensity of each calcite particle are randomly distributed, the birefringence brightness of different calcite particles varies randomly under the angular changes of 0°, 20°, and 45° that we have set. Therefore, it is possible to obtain an average HD close to the ideal value, resulting in a multi-level PUF label with independently encoded layers at different angles. In this scenario, the encoding capacity is defined as $m \times C^n$, where $m$ represents the number of encoding layers within one period of birefringence intensity variation (e.g., 0°-45°). Here, $m$ is equal to 3, resulting in an encoding capacity of $3 \times 2^{25}$ ($\approx 1.0 \times 10^8$).

### 2.5. The Digital Encoding of PUFs in the Fluorescence Mode

The photoluminescence signals from the fluorescent molecules embedded in the calcites provide another reliable secure authentication mode for the PUF labels. We can generate fluorescent colors across different wavelength ranges using various excitation lights, enabling multi-channel output responses in the fluorescence mode. As illustrated in **Figure** 4a–c, the different fluorescent-colored calcites from the same PUF label can be independently visualized under different excitation lights. We coded the three fluorescent colors as three independent channels, pixelated the microscopy images, and reduced them to a size of 20 pixels × 20 pixels. Subsequently, we binarized these images (Figure 4d–f) and calculated the bit uniformity, uniqueness, and repeatability of the three-color fluorescent calcites. After analyzing 50 PUF labels, we obtained the following metrics: the blue channel exhibited a bit uniformity of 0.440, uniqueness of 0.496 (Figure 4g), and repeatability of 0.091 (Figure 4g,j). Similarly, the green channel exhibited a bit uniformity of 0.455, uniqueness of 0.498 (Figure 4h), and repeatability of 0.091 (Figure 4h,k). The red channel showed a bit uniformity of 0.468, uniqueness of 0.500 (Figure 4i), and repeatability of 0.007 (Figure 4i,l). All these values fall within the ideal range, indicating that the three fluorescent colors can function independently as separate channels for authenticating PUF labels in fluorescence mode. Similar to the angle-dependent birefringence responses, the coding capacity in this mode can reach up to $k \times C^n$, where $k$ refers to the number of encoding channels. Hence, the coding capacity in three-channel fluorescence mode is $3 \times 2^{400}$ ($\approx 7.75 \times 10^{120}$).

Further, by simultaneously exciting and recording the blue, green, and red fluorescence, we combined the three RGB channels to obtain a color PUF readout (Figure 4m). Each pixel is encoded with three bits corresponding to the red, green, and blue fluorescence channels. With each bit assigned a value of 1 or 0 based on the fluorescent intensity of the corresponding color channel, there are a total of 8 coding combinations per pixel (Table S2, Supporting Information). Thus, the fluorescence image can be converted into a 3-bit color image (or 8-valued image) (Figure 4n) that can be used for more complex authentication purposes. In this case, the PUF labels continue to demonstrate strong performance in that the values of inter-HD and intra-HD are close to their respective ideal values (Figure 4o). The coding capacity in this scene is $C^s$, where $s$ represents the degrees of freedom. Here, degrees of freedom $s$ ($s = \mu(1-\mu)/\sigma^2$, where $\mu$ is the average inter-HD and $\sigma$ is the standard deviation) is used to denote the number of independent pixels since pixel points are not completely independent. As such, the coding capacity in this 8-valued fluorescent coding is $8^{213.4}$ ($\approx 5.24 \times 10^{192}$). This channel combination equips the PUF system with a higher coding capacity, enabling it to accommodate more complex application scenarios.

### 2.6. Authentication of the PUF Labels using Neural Networks

Since the PUFs with three RGB channels under fluorescence mode can be readily read out using a camera, a deep learning-based image recognition system is suitable for label authentication. Using a deep learning (DL) model for the image recognition of PUF labels can significantly reduce the complexity and speed up the recognition process by automation without losing accuracy.[14a,18,41] We employed convolutional neural networks (CNNs), a supervised branch of DL, to accomplish the image recognition of PUF labels (**Figure** 5a). We created 10 PUF labels as the authentic ones. We used a macro-lens-equipped camera to image each PUF label under a 365 nm UV flashlight 40 times under various lighting conditions and imaging angles (Figure S11, Supporting Information). Our image set contains 400 images labeled by 10 categories, a-j, corresponding to the 10 authentic PUF labels (Figure S12, Supporting Information). After training, the accuracy of the model reached 97.5% with a reasonable loss value (Figure 5b).

Once the DL model was constructed, we tested its ability to identify authentic PUF labels and distinguish them from ones

of the HDs between two arbitrary PUF labels in two measurements. The fabricated labels are nearly uncorrelated with each other. h) Schematics and the corresponding microscopy images of the PUF label captured under varying angles between the PUF label and the orthogonal polarizers. i) (Top) The microscopy images captured under the angles between the orthogonal polarizers angle and the sample of 0°, 20°, and 45°. (Bottom) The corresponding binary codes (5 pixels × 5 pixels). Scale bars: 100 µm. j) Bit uniformity of the multi-level encoding based on angular-dependent birefringence intensity. The average value is 0.4627. k) HDs of the multi-level PUF labels. The average value is 0.4507 and the standard deviation is 0.0853. Curves in (f) and (k) are fit to a Gaussian distribution.

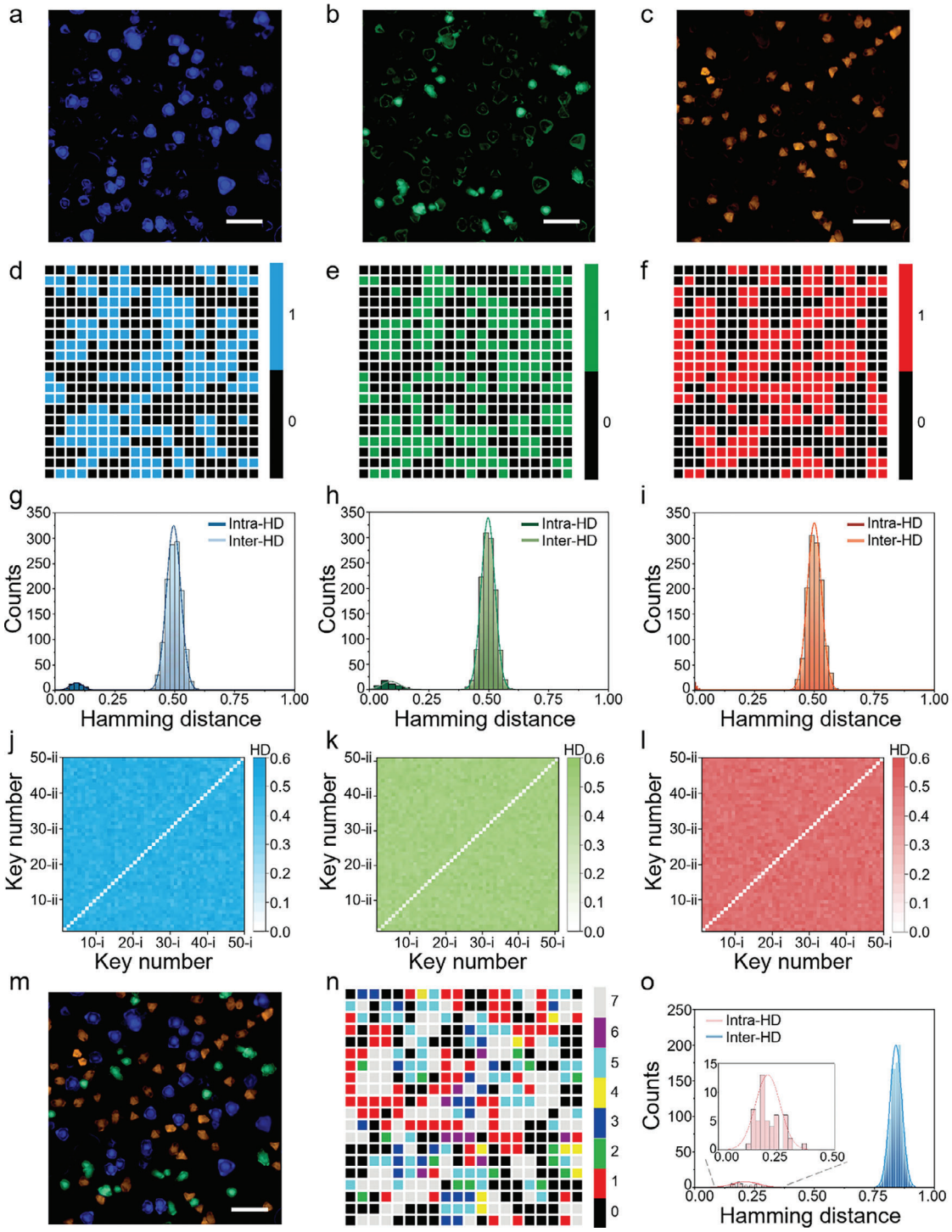


**Figure 4.** Encoding of PUF labels in the fluorescence mode. a–c) Fluorescence microscopy images of one PUF label under excitation wavelengths of 358 a), 488 b), and 550 c) nm, respectively. Scale bars: 200 µm. d–f) The corresponding 2D binary image encoding matrix based on the fluorescence microscopy images (resolution: 20 pixels × 20 pixels). g–i) The corresponding HDs generated from 50 labels. g) The average inter-HD is 0.496 with a standard deviation of 0.030, while the average intra-HD is 0.091 with a standard deviation of 0.027. h) The average inter-HD is 0.498 with a standard deviation of 0.029, while the average intra-HD is 0.091 with a standard deviation of 0.037. i) The average inter-HD is 0.500 with a standard deviation of 0.030, while the average intra-HD is 0.007 with a standard deviation of 0.006. j–l) Pairwise comparisons of 50 different PUF labels for the first and second measurements. m) Fluorescence microscopy images under the combined excitation wavelengths of 358, 488, and 550 nm. Scale bar: 200 µm. n) Corresponding 3-bit (or 8-valued) color image. o) The HDs of 8-valued coding. The average inter-HD is 0.8399 with a standard deviation of 0.0251 (ideal value: 0.875). The average intra-HD is 0.2128 with a standard deviation of 0.0531 (ideal value: 0).

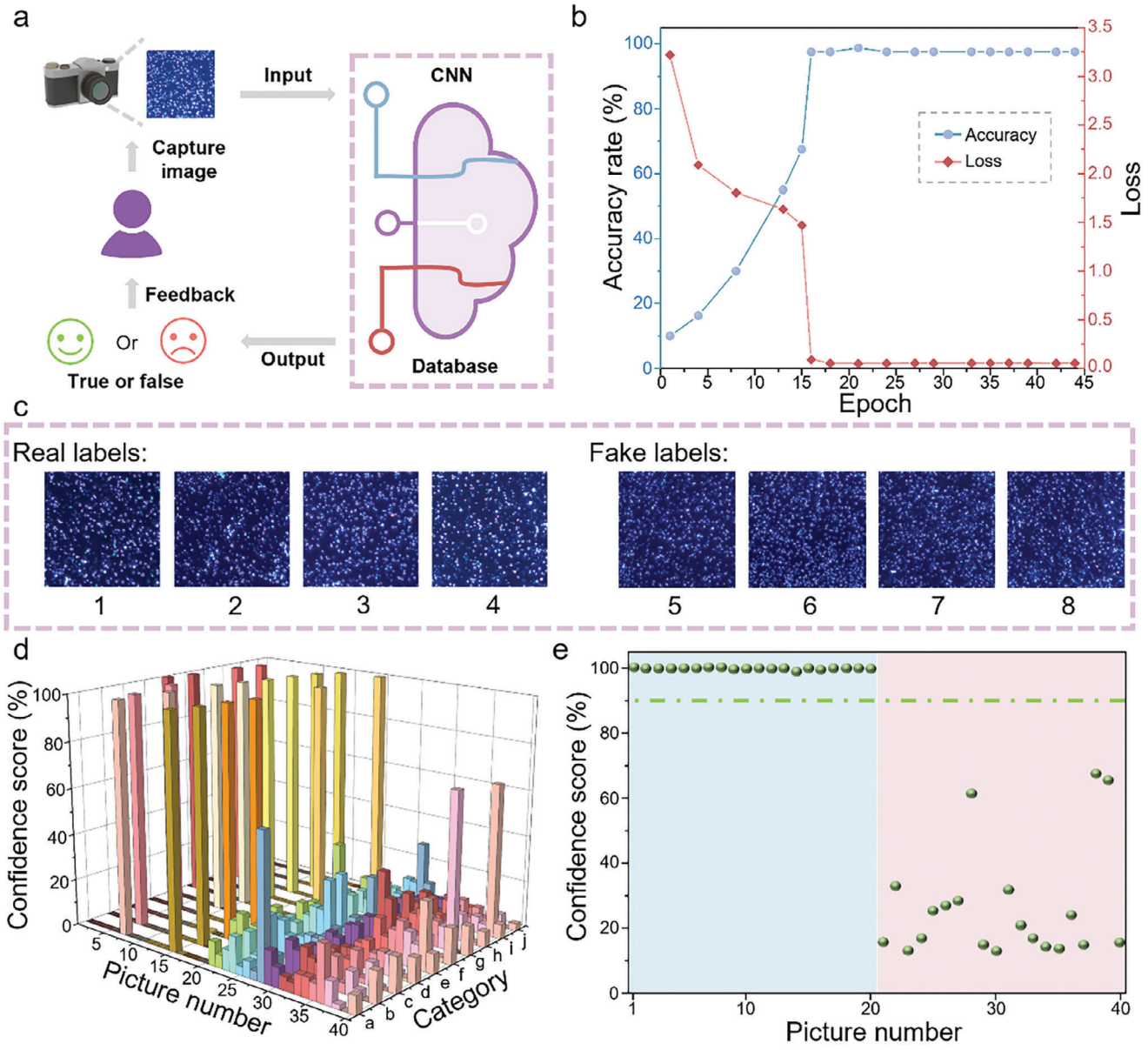


**Figure 5.** CNN-based authentication system. a) Schematic of the authentication flow diagram. Consumers input a label image into a DL model, which recognizes the image and returns a confidence score. If the score exceeds a threshold, the label is real; otherwise, it's fake. b) DL model accuracy rate and loss. The recognition accuracy reached its maximum value within 27 training epochs (it is related to the number of iterations per epoch and the amount of data information) and maintained consistently stable thereafter. c)A set of data for testing the image recognition function of the model. Pictures 1 to 4 belong to categories e, f, h, and i in the database, while pictures 5 to 8 are the fake labels from outside the database. d) The confidence score of each image corresponding to each category in the database. e) The maximum confidence scores of each image. The green line is the threshold value of the recognition rate.

that the model has not trained. We tested a total of 40 images, consisting of 20 genuine labels from the database and 20 fake labels. Some of the probe images are shown in Figure 5c. By feeding the images into the DL model, we can obtain the confidence score of each image attributed to each category (Figure 5d). The confidence scores of genuine images 1 to 20 are close to 100%, which correctly falls under their category. Conversely, the confidence scores of fake images 21 to 40 are distributed across all categories, indicating that they do not belong to any of the authentic PUF labels. Figure 5e shows the maximum confidence scores of each image across all categories; notably, the confidence scores for all fake PUF images remain at a significantly lower level than authentic ones. By setting a confidence score threshold of 90% to classify the input images, the false positive rate of the DL model is zero, indicating no fake labels were identified as authentic; at the same time, all authentic labels are correctly identified. The results affirm that the developed DL model can effectively discriminate between images of genuine and fake PUF labels, showcasing its efficiency, reliability, and adaptability in authenticating complex PUF patterns presented here.

It is important to note that we can improve the recognition efficiency by adjusting the model parameters and output format. Additionally, we are capable of scaling the database as the number of samples increases. To demonstrate this, we expanded the database to include 50 PUF labels, totaling 2000 images. In this expanded test, the output was simplified to display only the recognition confidence score, omitting the specific category of each image. We randomly selected 100 real images and 100 fake images for recognition. The results demonstrate that the model exhibits an excellent image recognition performance (Figure S13, Supporting Information), with each image taking less than 1 s to process.

### 2.7. Multiform Applications of the PUF Labels

At present, the PUF technology has not yet formed a fully mature commercialization system. One limitation is the need for bulky and costly detection equipment. Other limitations are intrinsic to the materials, such as complex preparation processes or inherent toxicity, as well as strict conditions of use. The calcite-based PUF labels we report in this work can be validated using a standard camera or portable microscope, overcoming the limitations posed by the availability of detection equipment and meeting the requirements of versatile application scenarios. In addition to providing straightforward yet diverse identification ways, our PUF labels offer notable advantages such as their low production cost, robustness, flexible manufacturing and usage, and soft and biodegradable substrate, making them an ideal solution for sustainable and secure authentication in various applications.

The conceptual schematic of the product authentication flow, as shown in **Figure** 6a, illustrates the three flows from the perspectives of PUF manufacturers, commodity producers, and consumers. i) On the PUF manufacturer's side, after manufacturing the PUF labels, these labels undergo testing under different modes, and the resulting readouts are uploaded as digital keys to a cloud database. Manufacturers can establish either a single certification model or a combination of multiple certification models, depending on the diverse needs of commodity producers. The PUF manufacturers should maintain the cloud database containing the encoding information and the certification system, allowing for efficient verification. ii) On the commodity producer's side, they customize PUF labels according to the commodity's value. Subsequently, the labels are securely attached to the products. iii) On the consumer's side, consumers purchase the commodities with the tested PUF labels attached. Consumers image the PUF labels using a digital camera or portable microscope to access cloud databases. The verification system recognizes the uploaded images of PUF labels and determines if they correspond to any of the tested PUF labels in the cloud database. Instant feedback will be provided on the authenticity of the products. This three-line approach ensures information security and benefits PUF manufacturers, commodity producers, and consumers. It effectively reduces the risk of fraud and counterfeit products while enhancing consumer trust and satisfaction. However, despite the effectiveness of our PUF labels in mitigating counterfeiting and forgery, the PUF database itself remains vulnerable to cyberattacks.[13b] If the database is compromised, the anti-counterfeiting effectiveness of all PUF labels would be invalid. While our study does not address this issue, we remain hopeful that future technological advancements will lead to the development of effective solutions to overcome this challenge.

Practically, besides necessitating excellent performance and simple detection methods, PUFs are also required to have a low cost and demonstrate robustness under various environmental conditions. Benefiting from the use of low-cost materials and the absence of large, complex equipment, the cost of a single calcite PUF can be as low as US$ 0.00226 per square millimeter, making calcite PUFs an economically viable solution for practical anticounterfeiting applications (Note S3, Supporting Information). To assess the robustness of the PUFs, we evaluated their stability against high temperature, mechanical force, deep UV light, high humidity, and heavy metal ions. The thermal stability of the PUF label was first tested under harsh conditions at 200 °C for 24 hours (Figure 6b). We compared the output responses in the birefringence mode before and after thermal treatment, and the average coincidence rate (the similarity of encoding matrix before and after treatment) is 92.45% (Figure 6d), indicating excellent readout stability under high temperatures. To ensure long-term reliable operation, PUF labels must also be mechanically robust to withstand external disruptions caused by unintended physical contact. To test this stability, we repeatedly applied and removed commercial medical tape to and from the calcite side of PUF labels 10 times (Figure 6c). Comparing the output responses before and after the tape pasting, we found that the average coincidence rate is 83.76% (Figure 6e), demonstrating sufficient mechanical stability to meet certain requirements during use. Additionally, The PUF labels exhibit resistance to deep UV light (254 nm, 10 W) exposure and can adapt to high-humidity environments. Their performance remains essentially unchanged after exposure to deep UV light for 10 hours or placement under 70–80% humidity for 1 month. Furthermore, the PUF labels maintain strong fluorescent signals even after treatment with heavy metal ions, such as copper nitrate—a commonly used fluorescence quenching agent—due to the dense and rigid crystal structure of the calcites (Figure S14, Supporting Information).

In practical application scenarios, PUFs also need to possess the ability to contact with various target surfaces conformally. Thanks to silk proteins' flexibility and outstanding adhesion properties, our constructed PUFs are well-equipped with this capability. More importantly, the flexibility of the imprinting technique employed here enables us to manipulate the distribution of disordered calcite arrays on the silk film's surface in various ways. This, in turn, facilitates the production of patterned PUF labels of different forms. Figure 6f–h illustrates the flexible application of a patterned PUF label on various target surfaces. Our PUF labels can be easily applied to the surface of calligraphy and paintings, serving as an effective tool to validate the authenticity and values of these commodities (Figure 6f). In this scenario, a patterned PUF label, depicting the character "王" in the seal script font, was created. This pattern is visible under natural light (Figure 6f-i), orthogonally polarized light (Figure 6f-ii), and UV light (Figure 6i-①), providing both signature and anti-counterfeiting functions. Taking advantage of the intrinsic biodegradable, food-grade quality, and flexibility of silk film, our PUF labels can be safely and stably used on agricultural products (Figure 6g). Here, a patterned PUF label featuring a four-leaf clover pattern that is invisible under natural light

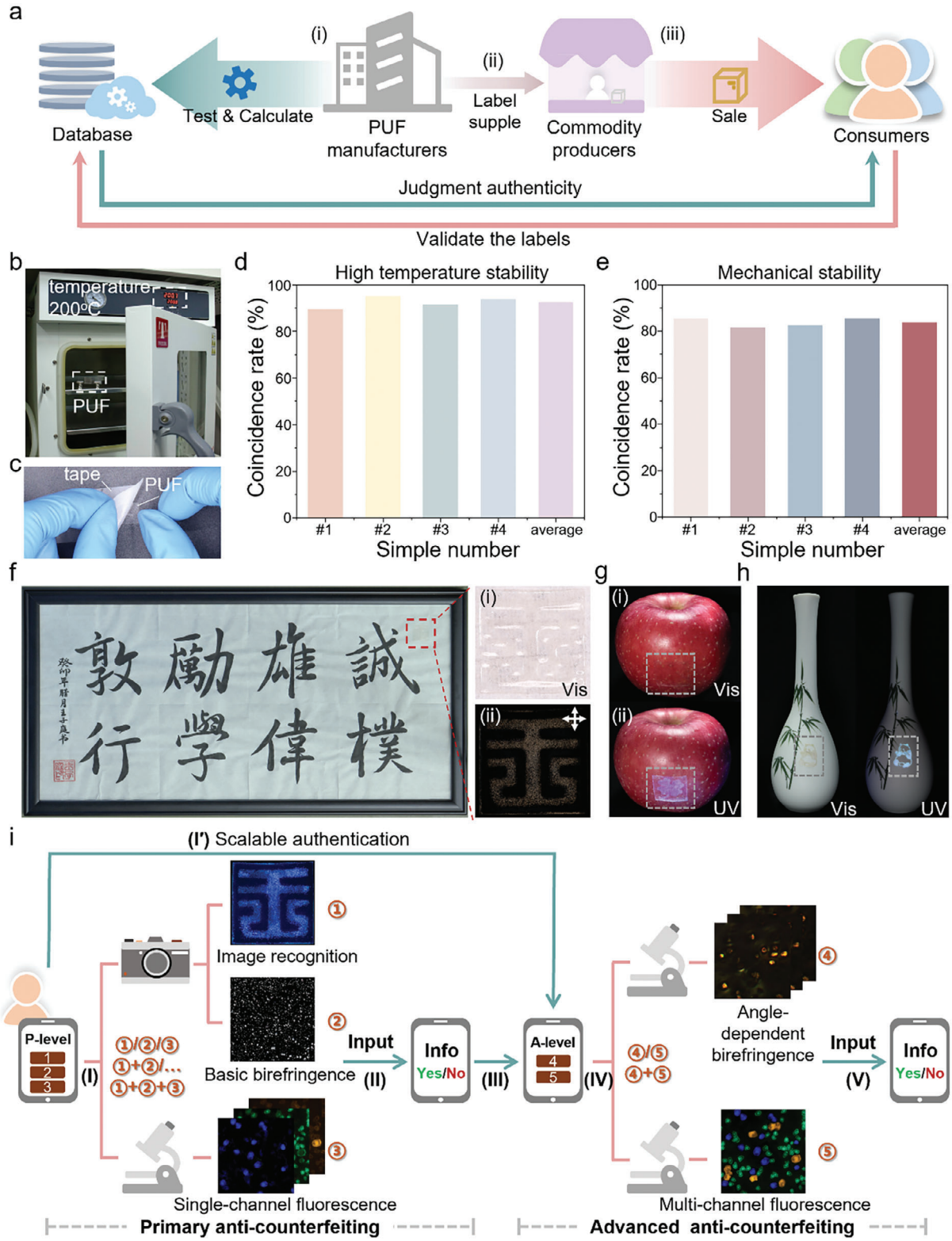


**Figure 6.** Stability, degradability, and application of the PUF labels. a) A conceptual schematic of the product's authentical flow. The process is divided into three parts: i) PUF manufacturers produce and test the PUF labels, and then store the information in a cloud database. ii) The commodity producers customize PUF labels and attach them to the products. iii) The tested PUF labels reach the consumers along with the commodities. Consumers scan the PUF labels to access the cloud database and then get the authenticity of the commodities. b,d) Thermal stability test for a PUF label (b) and the variation in encoding matrix after high-temperature treatment (d). c,e) Mechanical stability test for a PUF label (c) and the variation in encoding matrix

(Figure 6g-i) but becomes visible under UV light (Figure 6g-ii) is employed (see experimental section for details). Introducing concealable pattern information in PUF labels will further enhance the complexity of anti-counterfeiting measures and elevate the level of security. It is noteworthy that these PUF labels are produced without the use of hazardous materials, ensuring that no harmful residues affect the agricultural products' quality or safety. One can fix the PUF label to the surface of the agricultural products using a highly concentrated silk fibroin solution as an adhesive, which is non-toxic and water-soluble. Before consuming the agricultural products, the silk fibroin adhesive layer can be easily washed away with water to remove the PUF label. Furthermore, the imprinting approach can be combined with the kirigami technique to produce patterned PUF labels with complex designs, as exemplified by a panda pattern applied on a vase (Figure 6h).

In addition to meeting basic application requirements, the practicality of PUF labels must be carefully considered. Integrating multiple authentication technologies within a single PUF label significantly increases the overall complexity and security of the PUF labels, making them more challenging and costly for counterfeiters to replicate or clone. In the meantime, forming a multi-authentication, multi-level PUF system also enhances its utility in several important ways, including enabling customized authentication, flexible access, adaptive authentication, fault tolerance, and scalability (see Note S4, Supporting Information, for details). To demonstrate this, we summarized the PUF label's multiform applications by taking the label with a "王" pattern in Figure 6f as an example. As shown in Figure 6i, the whole anti-counterfeiting system can be divided into two parts: primary anti-counterfeiting (P-level), and advanced anti-counterfeiting (A-level). The P-level consists of three simple forms of authentication: image recognition, basic birefringence, and single-channel fluorescence recognition. During the authentication, consumers select one or more modes of P-level within the system based on the conditions outlined in Note S4, items 1 to 4 (Supporting Information), capture images (Figure 6i-I), and input these images to complete the primary authentication (Figure 6i-II). At this stage, authentication can terminate or proceed to the further A-level according to product requirements (Figure 6i-III). The A-level comprises two complex forms of authentication: angle-dependent birefringence and multi-channel fluorescence recognition. The A-level stage can only be accessed upon successful completion of the P-level authentication. The verification steps for the A-level are similar to those for the P-level (Figure 6i-IV,V). The authenticity of the product can only be guaranteed if the required authentication is passed. In the condition of needing scalable authentication systems with the growth of security (Note S4, item 5, Supporting Information), the A-level can be automatically activated by the system to replace the P-level (Figure 6i-I'), thus completing the update iteration. In all, by leveraging the strengths of different technologies, the calcite PUF label delivers a more secure, flexible, and reliable authentication system applicable to diverse scenarios.

Last but not least, the environmentally friendly composition of the PUFs, comprising natural minerals, bio-dyes, and natural polymers, makes them non-polluting to the environment. Benefiting from the high biodegradability of silk protein, these PUF labels can degrade rapidly in natural environments. As depicted in Figure S15 (Supporting Information), the PUF labels undergo a disintegrated process within 62 days when exposed to a humid soil environment at room temperature, due to the presence of microorganisms capable of directly attacking and digesting the silk protein chains. It is important to highlight that while calcium carbonate itself is not biodegradable in the sense that organic materials like silk proteins are, certain microorganisms can contribute to the chemical breakdown of calcium carbonate through their acidic metabolites.[42] These metabolites facilitate the decomposition of calcium carbonate via indirect chemical processes. As a result, calcite used here can be considered biodegradable, as it doesn't accumulate in the environment in harmful ways. Instead, it can dissolve back into the natural carbon cycle. To illustrate that the degradation behavior of PUF labels is affected by the soil environment, such as pH levels, we investigated their acid degradation behavior. The results indicate that the PUF labels exhibit markedly different degradation rates in hydrochloric acid solutions of varying concentrations, with the degradation rate increasing as the acid concentration rises (Figure S16, Supporting Information). Based on these findings, a high-performance, simple-to-certify, yet environmentally friendly PUF label is achieved using all-biobased materials.

## 3. Conclusion

The combination of all-water-based biomimetic mineralization and imprinting techniques provides a green and effective approach for creating biodegradable, robust, reliable, and versatile PUF systems featuring multi-mode optical encoding, multi-level cryptographic keys, and multiple authentication operations. This platform overcomes the inherent limitations of traditional optical PUF labels, which require bulky and inaccessible equipment for authentication, by enabling rapid and convenient identification using only a digital camera or a portable microscope. Meanwhile, this all-biomaterial-based anti-counterfeiting system significantly enhances cryptographic capacity, complexity, and diversity while avoiding energy-intensive input, toxic byproducts, waste, environmental degradation, and biological incompatibility. These capacities, combined with the platform's robustness, multi-modal patternability, and co-conformal surface contact capability, make the PUF system particularly suitable for a wide range of product authentication and security applications related to human life and health, such as artificial organs, high-end

after tape pasting treatment (e). f) Application of a patterned PUF label to a calligraphy. The enlarged image shows the pattern information under natural light (i) and orthogonal polarized light (ii). g) Anti-counterfeiting of agricultural products. The pattern of the PUF label is invisible under natural light (i) but becomes visible under UV light (ii). h) Application of a kirigami PUF label to a vase. i) A summary of the label's multiform applications. I, II) Primary anti-counterfeiting (P-level). III-V) Advanced anti-counterfeiting (A-level). Consumers select the mode of P-level (I) or A-level (IV) and complete the image capture, then input the images into the system to complete authentication (II or V). III) The switch from P-level to A-level. I') Scalable authentication by activating or integrating A-level with the growth of security needs.

drugs, and implantable devices. There are significant opportunities to extend this strategy to other calcium carbonate crystal types or biomimetic mineral systems by leveraging the versatility of silk protein in mediating mineral crystallization.[37,43] By integrating multiple types of calcium carbonate crystals or various biomimetic mineral species into a single platform, we can significantly enhance the coding complexity and capacity, paving the way for more sophisticated and secure authentication solutions. In addition to fluorescent molecules, other light-responsive molecules such as photochromic and phosphorescent compounds can potentially be introduced into calcite crystals with the assistance of silk protein, thereby endowing the crystals with the appropriate optical functions. The capacity to incorporate functional components into the mineralization process opens up exciting possibilities for the future development of new green, multifunctional, and smart optical and information devices based on biominerals.

## 4. Experimental Section

*Silk Fibroin Solution Preparation*: The regenerated silk fibroin solution was extracted from the silk cocoons of the *Bombyx mori* silkworm using established protocols.[44] Briefly, the silk cocoons cut into small pieces were boiled in a solution of $Na_2CO_3$ (0.02 M) for 30 min and thoroughly washed with deionized water to remove the sericin. After drying under ambient air for 2 days, the degummed silk fibers were dissolved in a LiBr solution (9.3 M) at 60 °C for 4 hours. Following this, the dissolved silk fibroin was dialyzed in deionized water with dialysis bags (molecular-weight cutoff: 3500) for 3 days. The silk fibroin solution, with a concentration of ≈6-7 wt.%, was obtained by centrifuging at 11000 rpm for 20 min, followed by two rounds of filtration using dust-free paper.

*Crystallization of Calcites*: Before commencing the experiment, it is crucial to clean all glass products thoroughly. First, the beakers were cleaned and sonicated with absolute ethyl alcohol for 5–10 min. Subsequently, the cover glasses and beakers were soaked in a mixed solution of $H_2O$-$HNO_3$ (65%~68%)-$H_2O_2$ (30%) (1:1:1, v/v/v) for 12 h. Finally, the cover glasses and beakers were rinsed alternately with deionized water and acetone, and then dried in air and set aside for further use. Crystal growth was achieved using the carbon dioxide diffusion method described elsewhere.[35] Initially, the as-prepared silk solution was diluted to a concentration of 1 wt.%. An equal mass of $CaCl_2$ solution (20 mmol $L^{-1}$) was mixed with the diluted silk solution. Subsequently, three different fluorescent-colored commercial bio-dyes were individually added to the separate mixture and stirred well to ensure uniform distribution. Next, the cleaned cover glass was gently suspended on the liquid surface. The beakers were sealed with a parafilm, and six holes were punctured through the parafilm for $CO_2$ entry. In a separate beaker, 3 g of $(NH_4)_2CO_3$ was placed, sealed with parafilm, and similarly punctured with six holes. Finally, all the beakers were placed inside a desiccator (6.5 L), which was sealed with Vaseline to prevent $CO_2$ leakage. The setup was left undisturbed at room temperature for a certain time (48 hours, if not otherwise indicated). After this period, the cover glasses were removed and rinsed with deionized water. Once air-dried, one layer of randomly distributed calcite crystals was obtained on the surface of the cover glasses.

*Fabrication of the PUF Labels*: An amorphous silk film with a thickness of ≈100 µm was prepared to serve as a substrate for the PUF label. This was achieved by casting a specific volume of silk solution onto a silicon wafer treated with trichloro(1H,1H,2H,2H-perfluorooctyl) silane and allowing it to dry at ambient conditions overnight. The imprinting transfers of grown calcites from cover glasses to silk films were performed using the recently developed water vapor-assisted imprinting technique.[34] In brief, the prepared silk film was firmly attached to a clean PDMS substrate and then exposed to 45 °C water vapor in an electrically heated constant-temperature water bath (NK-420, Aipu, China) for 65 s. Following this treatment, the treated side of the silk film was quickly placed over the calcites grown on the cover glass. By applying pressure, the calcites were imprinted onto the silk film. Once the silk film dried, it was peeled off from the cover glass, completing one imprint cycle. This imprinting process was repeated three times to accomplish the transfer of different fluorescent calcite. For each subsequent imprint, the water vapor treatment time was increased by 5 s. Thus, a PUF label with randomly distributed calcite imprints on a silk substrate was successfully created.

*Characterization*: Optical microscopy images were captured using an optical microscope (DM2700 M, Leica, Germany). The morphologies of calcites were observed with a field emission scanning electron microscope (ULTRA 55, Zeiss, Germany) at a voltage of 5 kV and a current of 10 µA. The polymorph of $CaCO_3$ was determined by a Raman spectrometer (Thermo Scientific DXR, Thermo Fisher, America) with an excitation wavelength of 633 nm. The crystallographic analysis of calcite was assayed using an X-ray powder diffractometer (Smartlab SE, Rigaku, Japan). The thermal decomposition of the calcites was analyzed using a thermogravimetric analyzer (TG 209 F3 Tarsus, Netzsch, Germany). Birefringence microscope images were captured using a polarized optical microscope (DM2700 P, Leica, Germany). The fluorescence microscope images were captured using a fluorescence microscope (Axio Vert. A1, Zeiss, Germany), and the fluorescence spectra were measured using an Ultraviolet-vision-near infrared micro spectrometer (CRAIC 20/30PV, America). The stratified scanning of the fluorescent calcite was conducted under the transmission mode of a laser confocal microscope (FV3000, Olympus, Japan). The shooting device shown in Figure S5 (Supporting Information) involved the use of a digital camera (EOS 850D, Canon, Japan) equipped with a macro lens (105 mm F2.8 DG MACRO HSM, SIGMA, Japan), two commercial photographic polarizers (F-ND2K, JJC, China & XS-Pro1, Stppo, China), and a white light source. The polarization direction of the two polarizers was aligned vertically to acquire the birefringence signal. The shooting device in Figure S11 (Supporting Information) used for image recognition comprised a digital camera equipped with a macro lens, and a 365nm ultraviolet flashlight (V100, SHENYU, China).

*Readout and Digitization of the PUF Labels*: The PUF labels were read by 1) a digital camera equipped with a macro lens, 2) polarized optical microscopy, and 3) fluorescence microscopy. To ensure the precise positioning of each image acquisition, an alignment mark was set during the fabrication of the PUF label. This alignment mark is placed on the silk substrate outside the imprinted calcite arrays (Figure S17, Supporting Information), ensuring that it does not interfere with the PUF label's information. By identifying the position of the alignment mark and recording the horizontal distance (a) and vertical distance (b) from the recognition area to the center of the alignment mark, accurate positioning was consistently achieved for each image capture. Even if the PUF label is moved, the recognition area can still be reliably identified by referencing the position of the alignment mark. MATLAB (R2023a) codes were designed to extract, calculate, and analyze the data information from the captured images. During this process, the images were first converted to grayscale using the "rgb2gray" function. Then, the pixel size was set, established the appropriate threshold for each image using the "median" function, and binarized the image. The Hamming distance calculation was implemented by using the "xor" and "nnz" functions and the correlation coefficient calculation by using the "corr" function. Furthermore, The crucial metrics including the bit uniformity, uniqueness, and repeatability were analyzed according to the equations mentioned in the main text.

*Image Recognition*: All deep learning techniques utilized in this work were based on a convolutional neural network, executed within MATLAB (R2023a), using a GPU (GeForce RTX 4070 Ti) for calculations. The input images were resized to 404 × 404 × 3 for effective training. The database (Figure S12, Supporting Information) comprised 10 PUF labels, divided into 10 distinct categories, totaling 400 images. Of these, 70% of the images were randomly selected under each category as the training set and the remaining 30% as the validation set (i.e., 280 images were randomly designated as the training set, while the remaining 120 images served as the validation set). To train the model, images underwent convolution, pooling, and fully connected operations, followed by classification (Figure S18, Supporting Information). 100 epochs of training (no

overfitting occurred) were conducted, with validation results returned during each epoch, and repeated the training process until convergence. The total learning and verification process took 30 min. Upon completion of model training, users could input a random image into the model to verify its authenticity. The model would then accurately display the validation rate, providing a reliable indication of the image's authenticity.

*Stability Analysis of the PUF Label*: First, a macro-lens-equipped digital camera was used to capture the response of the PUF label in the birefringence mode and obtained its binary image. The PUF label was then subjected to various treatments: heated in a 200 °C oven for 24 h, repeatedly attached and detached using commercial medical tapes, exposed to deep UV light (254 nm, 10 W) for 10 hours, or placed in a high-humidity chamber (70–80% RH) for one month. After each treatment, the binary image of the PUF label was captured again. The binary images were analyzed before and after the treatments to determine their similarity. Each process was repeated on four PUF labels, and the average similarity was calculated to assess the coincidence rate of the PUF labels under various extreme conditions.

*Patterning of the PUF Labels*:

1) PUF label with a seal script font "王" pattern: This patterned label was created by using a stencil during the imprinting transfer process. First, a polydimethylsiloxane (PDMS) stencil with the desired pattern, created using a $CO_2$ laser cutter (SIR-2075; Trotec), was applied to a silk film that was affixed to a clean PDMS substrate. The stencil-covered silk film was then subjected to water vapor treatment at 45 °C for 65 s. After the treatment, the stencil was removed, and the treated side of the silk film was quickly placed over the calcites grown on the cover glass. By applying pressure, the calcites were imprinted onto the silk film. Due to the presence of the PDMS pattern stencil, the part covered by the stencil had not been treated with water vapor, thus failing to imprint the calcites. In contrast, the exposed areas of the silk film had been treated, allowing the silk protein molecular chains to move sufficiently to enable imprinting. Once the silk film dried, it was peeled off from the cover glass, completing one imprint cycle. This imprinting process was repeated three times to achieve the transfer of different fluorescent calcite. For each subsequent imprint, the PDMS stencil was positioned in the same location as the previous time. Therefore, the PUF label with a seal script font "王" pattern was successfully built.
2) PUF label with a four-leaf clover pattern: In this experiment, we need to first obtain a four-leaf clover pattern of calcites on a cover glass grown with blue fluorescent calcites using the imprinting transfer method. For this purpose, a PDMS template was covered in the shape of a four-leaf clover with a piece of silk film. After treating the silk film with water vapor and performing the imprinting process, the calcites located outside the four-leaf clover pattern were transferred, resulting in a distinct four-leaf clover pattern on the coverslip. Following this step, the four-leaf clover pattern was transferred on the coverslip using another piece of silk film prepared for PUF labeling. After that, green and red fluorescent calcites were sequentially transferred on this film without the aid of any mask and finally realized the production of patterned PUF labels.
3) PUF label with a kirigami pattern: A commercial $CO_2$ laser cutter was used directly on the calcite-decorated silk film for the cutting process. The laser power intensity was set to 4% of the maximum energy, with a fixed speed of 1 step $s^{-1}$.

## Supporting Information

Supporting Information is available from the Wiley Online Library or from the author.

## Acknowledgements

This work was supported by the National Key R&D Program of China (No.2021YFA1202000, 2022YFA1203702), the National Natural Science Foundation of China (No. 62175102), the Natural Science Foundation of Jiangsu Province, Major Project (No. BK20212004), and the Program for Innovative Talents and Entrepreneurs in Jiangsu (No. JSSCTD202138).

## Conflict of Interest

The authors declare no conflict of interest.

## Author Contributions

Y.W. and Z.-T.W. conceived the idea and designed the research. Z.-T.W. and Y.-H.F. performed research. All authors contributed to the data analysis. Z.-T.W., M.L., Y.W., and Y.-Q.L. wrote the manuscript. Y.W. and Y.-Q.L. supervised the research.

## Data Availability Statement

The data that support the findings of this study are available from the corresponding author upon reasonable request.

## Keywords

anticounterfeit, biomimetic mineralization, calcite, physical unclonable function, silk protein

Received: June 26, 2024
Revised: October 1, 2024
Published online: December 2, 2024

[1] a) R. V. Solms, J. V. Niekerk, *Computers & Security* **2013**, *38*, 97; b) O. I. Abiodun, E. O. Abiodun, M. Alawida, R. S. Alkhawaldeh, H. Arshad, *Wireless Pers. Commun.* **2021**, *119*, 2603; c) A. E. Omolara, A. Alabdulatif, O. I. Abiodun, M. Alawida, A. Alabdulatif, W. H. Alshoura, H. Arshad, *Computers & Security* **2022**, *112*, 102494.
[2] a) P. Aldhous, *Nature* **2005**, *434*, 132; b) E. L. Prime, D. H. Solomon, *Angew. Chem.-Int. Edit.* **2010**, *49*, 3726; c) H. Nili, G. C. Adam, B. Hoskins, M. Prezioso, J. Kim, M. R. Mahmoodi, F. M. Bayat, O. Kavehei, D. B. Strukov, *Nat. Electron.* **2018**, *1*, 197; d) A. Esidir, N. Kayaci, N. B. Kiremitler, M. Kalay, F. Sahin, G. Sezer, M. Kaya, M. S. Onses, *ACS Appl. Mater. Interfaces* **2023**, *15*, 41373; e) H. Sun, S. Maji, A. P. Chandrakasan, B. Marelli, *Sci. Adv.* **2023**, *9*, eadf1978.
[3] a) K. T. P. Lim, H. L. Liu, Y. J. Liu, J. K. W. Yang, *Nat. Commun.* **2019**, *10*, 25; b) I. Kim, J. Jang, G. Kim, J. Lee, T. Badloe, J. Mun, J. Rho, *Nat. Commun.* **2021**, *12*, 3614; c) J. T. Gong, L. X. Xiong, M. B. Pu, X. Li, X. L. Ma, X. G. Luo, *Adv. Sci.* **2024**, *11*, 2308687.
[4] a) W. Hong, Z. K. Yuan, X. D. Chen, *Small* **2020**, *16*, 1907626; b) X. T. Lai, Q. Ren, F. Vogelbacher, W. E. I. Sha, X. Y. Hou, X. Yao, Y. L. Song, M. Z. Li, *Adv. Mater.* **2022**, *34*, 2107243; c) N. Dalloz, V. D. Le, M. Hebert, B. Eles, M. A. F. Figueroa, C. Hubert, H. F. Ma, N. Sharma, F. Vocanson, S. Ayala, N. Destouches, *Adv. Mater.* **2022**, *34*, 2104054.
[5] a) S. Huang, J. K. Wu, *IEEE Trans. Inf. Forensic Secur.* **2007**, *2*, 164; b) H. J. Jeon, J. W. Leem, Y. Ji, S. M. Park, J. Park, K. Y. Kim, S. W. Kim, Y. L. Kim, *Adv. Funct. Mater.* **2022**, *32*, 2112479.
[6] a) C. Y. Zhang, B. Wang, W. B. Li, S. Q. Huang, L. Kong, Z. C. Li, L. Li, *Nat. Commun.* **2017**, *8*, 1138; b) X. W. Yu, H. Y. Zhang, J. H. Yu, *Aggregate* **2021**, *2*, 20.
[7] a) D. Taylor, *J. Med. Syst.* **2014**, *38*, 141; b) G. Khalil, R. Doss, M. Chowdhury, *J. Sens. Actuar. Netw.* **2019**, *8*, 37.

[8] a) R. Pappu, R. Recht, J. Taylor, N. Gershenfeld, *Science* **2002**, *297*, 2026; b) Z. Y. Hu, J. Comeras, H. Park, J. S. Tang, A. Afzali, G. S. Tulevski, J. B. Hannon, M. Liehr, S. J. Han, *Nat. Nanotechnol.* **2016**, *11*, 559; c) Y. S. Gao, S. F. Al-Sarawi, D. Abbott, *Nat. Electron.* **2020**, *3*, 81.
[9] R. Arppe, T. J. Sørensen, *Nat. Rev. Chem.* **2017**, *1*, 0031.
[10] a) A. Chen, *IEEE Electron Device Lett.* **2015**, *36*, 138; b) B. Gao, B. H. Lin, Y. C. Pang, F. Xu, Y. Y. Lu, Y. C. Chiu, Z. W. Liu, J. S. Tang, M. F. Chang, H. Qian, H. Q. Wu, *Sci. Adv.* **2022**, *8*, eabn7753; c) M. Y. Yang, Z. L. Ye, H. Y. Pan, M. Farhat, A. E. Cetin, P. Y. Chen, *Sci. Adv.* **2023**, *9*, eadg7481.
[11] a) Y. Q. Gu, C. He, Y. Q. Zhang, L. Lin, B. D. Thackray, J. Ye, *Nat. Commun.* **2020**, *11*, 516; b) T. T. Zhang, L. Z. Wang, J. Wang, Z. Q. Wang, M. Gupta, X. Y. Guo, Y. Zhu, Y. C. Yiu, T. K. C. Hui, Y. Zhou, C. Li, D. Y. Lei, K. H. Li, X. Q. Wang, Q. Wang, L. Shao, Z. Q. Chu, *Nat. Commun.* **2023**, *14*, 2507.
[12] a) H. M. Chen, M. Song, Z. Guo, R. F. Li, Q. M. Zou, S. J. Luo, S. Zhang, Q. Luo, J. Hong, L. You, *Nano Lett.* **2018**, *18*, 7211; b) S. Lee, J. Kang, J. M. Kim, N. Kim, D. Han, T. Lee, S. Ko, J. Yang, S. Lee, S. Lee, D. Koh, M. G. Kang, J. Lee, S. Noh, H. Lee, J. Kwon, S. H. C. Baek, K. J. Kim, B. G. Park, *Adv. Mater.* **2022**, *34*, 2203558.
[13] a) Y. Li, M. M. Bidmeshki, T. Kang, C. M. Nowak, Y. Makris, L. Bleris, *Sci. Adv.* **2022**, *8*, eabm4106; b) A. M. Luescher, A. L. Gimpel, W. J. Stark, R. Heckel, R. N. Grass, *Nat. Commun.* **2024**, *15*, 2955.
[14] a) Y. Liu, F. Han, F. S. Li, Y. Zhao, M. S. Chen, Z. W. Xu, X. Zheng, H. L. Hu, J. M. Yao, T. L. Guo, W. Z. Lin, Y. H. Zheng, B. G. You, P. Liu, Y. Li, L. Qian, *Nat. Commun.* **2019**, *10*, 2409; b) H. Im, J. Yoon, B. So, J. Choi, D. H. Park, S. Kim, W. Park, *ACS Nano* **2024**, *18*, 11703.
[15] X. F. Lin, D. X. Shi, G. B. Yi, D. S. Yu, *Responsive Mater.* **2024**, *2*, e20230031.
[16] A. Anastasiou, E. I. Zacharaki, A. Tsakas, K. Moustakas, D. Alexandropoulos, *Sci. Rep.* **2022**, *12*, 2891.
[17] J. H. Kim, S. Jeon, J. H. In, S. Nam, H. M. Jin, K. H. Han, G. G. Yang, H. J. Choi, K. M. Kim, J. Shin, S. W. Son, S. J. Kwon, B. H. Kim, S. O. Kim, *Nat. Electron.* **2022**, *5*, 539.
[18] J. Y. Wang, Q. Zhang, R. Z. Chen, J. Li, J. H. Wang, G. Y. Hu, M. Y. Cui, X. Jiang, B. Song, Y. He, *Nano Today* **2021**, *41*, 101324.
[19] Q. Li, F. L. Chen, J. B. Kang, J. Su, F. Huang, P. D. Wang, X. Yang, Y. D. Hou, *Adv. Funct. Mater.* **2021**, *31*, 2010537.
[20] J. F. Zhang, Y. X. Liu, C. Njel, S. Ronneberger, N. V. Tarakina, F. F. Loeffler, *Nat. Nanotechnol.* **2023**, *18*, 1027.
[21] Z. Q. Man, C. Y. Dong, J. Bian, Z. D. Lu, Y. Q. Lu, W. H. Zhang, *Nano Lett.* **2024**, *23*, 7019.
[22] H. Guo, Y. Qin, Z. B. Wang, Y. X. Ma, H. F. Wen, Z. H. Li, Z. M. Ma, X. Li, J. Tang, J. Liu, *Adv. Funct. Mater.* **2024**, *34*, 2304648.
[23] a) K. Kim, S. U. Kim, M. Y. Choi, M. H. Saeed, Y. Kim, J. H. Na, *Light Sci. Appl.* **2023**, *12*, 245; b) S. Nocentini, U. Rüehrmair, M. Barni, D. S. Wiersma, F. Riboli, *Nat. Mater.* **2024**, *23*, 369.
[24] a) J. W. Leem, M. S. Kim, S. H. Choi, S. R. Kim, S. W. Kim, Y. M. Song, R. J. Young, Y. L. Kim, *Nat. Commun.* **2020**, *11*, 328; b) Y. Q. Fan, C. H. Zhang, Z. H. Gao, W. Zhou, Y. Hou, Z. H. Zhou, J. N. Yao, Y. S. Zhao, *Adv. Mater.* **2021**, *33*, 2102586.
[25] S. M. Park, G. Park, D. K. Yoon, *Adv. Mater.* **2023**, *35*, 2370250.
[26] Y. Kim, J. Lim, J. H. Lim, E. Hwang, H. Lee, M. Kim, I. Ha, H. Cho, J. Kwon, J. Oh, S. H. Ko, H. Pan, S. Hong, *Adv. Mater.* **2023**, *35*, 2212294.
[27] a) Y. W. Hu, T. P. Zhang, C. F. Wang, K. K. Liu, Y. Sun, L. Li, C. F. Lv, Y. C. Liang, F. H. Jiao, W. B. Zhao, L. Dong, C. X. Shan, *Adv. Funct. Mater.* **2021**, *31*, 2102108; b) M. S. Kim, G. J. Lee, J. W. Leem, S. Choi, Y. L. Kim, Y. M. Song, *Nat. Commun.* **2022**, *13*, 247; c) F. H. Jiao, C. N. Lin, L. Dong, X. Mao, Y. Wu, F. Y. Dong, Z. F. Zhang, J. L. Sun, S. F. Li, X. Yang, K. K. Liu, L. J. Wang, C. X. Shan, *Adv. Sci.* **2024**, *11*, 2308337.
[28] a) G. Falini, S. Albeck, S. Weiner, L. Addadi, *Science* **1996**, *271*, 67; b) Y. Politi, T. Arad, E. Klein, S. Weiner, L. Addadi, *Science* **2004**, *306*, 1161; c) A. B. Rodríguez-Navarro, P. Marie, Y. Nys, M. T. Hincke, J. Gautron, *J. Struct. Biol.* **2015**, *190*, 291.
[29] a) M. Cusack, A. Freer, *Chem. Rev.* **2008**, *108*, 4433; b) P. Gilbert, K. D. Bergmann, N. Boekelheide, S. Tambutté, T. Mass, F. Marin, J. F. Adkins, J. Erez, B. Gilbert, V. Knutson, M. Cantine, J. O. Hernández, A. H. Knoll, *Sci. Adv.* **2022**, *8*, eabl9653.
[30] a) R. N. Smartt, W. H. Steel, *J. Opt. Soc. Am.* **1959**, *49*, 710; b) O. S. Pokrovsky, J. Schott, *Environ. Sci. Technol.* **2002**, *36*, 426; c) Z. F. Deng, L. N. Chen, L. Li, *J. Mech. Behav. Biomed. Mater.* **2023**, *137*, 105538.
[31] a) A. S. Finnemore, M. R. J. Scherer, R. Langford, S. Mahajan, S. Ludwigs, F. C. Meldrum, U. Steiner, *Adv. Mater.* **2009**, *21*, 3928; b) Y. Y. Kim, C. L. Freeman, X. Q. Gong, M. A. Levenstein, Y. W. Wang, A. Kulak, C. Anduix-Canto, P. A. Lee, S. B. Li, L. Chen, H. K. Christenson, F. C. Meldrum, *Angew. Chem., Int. Ed.* **2017**, *56*, 11885.
[32] a) Y. Y. Kim, K. Ganesan, P. C. Yang, A. N. Kulak, S. Borukhin, S. Pechook, L. Ribeiro, R. Kröger, S. J. Eichhorn, S. P. Armes, B. Pokroy, F. C. Meldrum, *Nat. Mater.* **2011**, *10*, 890; b) W. Hao, D. Porter, Z. Z. Shao, *RSC Adv.* **2014**, *4*, 35258.
[33] a) Y. J. Liu, H. D. Zang, L. Wang, W. F. Fu, W. T. Yuan, J. K. Wu, X. Y. Jin, J. S. Han, C. F. Wu, Y. Wang, H. L. L. Xing, H. Z. Chen, H. Y. Li, *Chem. Mater.* **2016**, *28*, 7537; b) B. Marzec, D. C. Green, M. A. Holden, A. S. Coté, J. Ihli, S. Khalid, A. Kulak, D. Walker, C. Tang, D. M. Duffy, Y. Y. Kim, F. C. Meldrum, *Angew. Chem., Int. Ed.* **2018**, *57*, 8623.
[34] C. Jiang, T. Wang, Y. H. Fu, P. Chen, G. M. Tao, Y. Wang, Y. Q. Lu, *Matter* **2024**, *7*, 1591.
[35] W. Hao, D. Porter, X. T. Wang, Z. Z. Shao, *CrystEngComm* **2014**, *16*, 9176.
[36] a) X. L. Zhang, Z. H. Fan, Q. Lu, Y. L. Huang, D. L. Kaplan, H. S. Zhu, *Acta Biomater.* **2013**, *9*, 6974; b) C. L. Xiao, M. Li, B. J. Wang, M. F. Liu, C. Y. Shao, H. H. Pan, Y. Lu, B. B. Xu, S. W. Li, D. Zhan, Y. Jiang, R. K. Tang, X. Y. Liu, H. Cölfen, *Nat. Commun.* **2017**, *8*, 1398.
[37] T. Wang, D. Porter, Z. Z. Shao, *Adv. Funct. Mater.* **2012**, *22*, 435.
[38] a) A. N. Kulak, P. Iddon, Y. T. Li, S. P. Armes, H. Cölfen, O. Paris, R. M. Wilson, F. C. Meldrum, *J. Am. Chem. Soc.* **2007**, *129*, 3729; b) R. Q. Song, A. W. Xu, M. Antonietti, H. Cölfen, *Angew. Chem.-Int. Edit.* **2009**, *48*, 395.
[39] a) C. Gabrielli, R. Jaouhari, S. Joiret, G. Maurin, *J. Raman Spectrosc.* **2000**, *31*, 497; b) C. Cheng, Z. Z. Shao, F. Vollrath, *Adv. Funct. Mater.* **2008**, *18*, 2172.
[40] S. J. Xu, P. Y. Wu, *CrystEngComm* **2013**, *15*, 5179.
[41] J. D. Smith, M. A. Reza, N. L. Smith, J. X. Gu, M. Ibrar, D. J. Crandall, S. E. Skrabalak, *ACS Nano* **2021**, *15*, 2901.
[42] a) C. Dupraz, P. T. Visscher, *Trends Microbiol.* **2005**, *13*, 429; b) D. M. Wang, X. Z. Yu, K. P. Xu, G. Q. Bi, M. Cao, E. Zelzion, C. X. Fu, P. P. Sun, Y. Liu, F. Kong, G. Y. Du, X. H. Tang, R. J. Yang, J. H. Wang, L. Tang, L. Wang, Y. J. Zhao, Y. Ge, Y. Y. Zhuang, Z. L. Mo, Y. Chen, T. Gao, X. W. Guan, R. Chen, W. H. Qu, B. Sun, D. Bhattacharya, Y. X. Mao, *Nat. Commun.* **2020**, *11*, 4028.
[43] a) Y. C. Li, Y. R. Cai, X. D. Kong, J. M. Yao, *Appl. Surf. Sci.* **2008**, *255*, 1681; b) X. Fei, W. Li, Z. Z. Shao, S. Seeger, D. Y. Zhao, X. Chen, *J. Am. Chem. Soc.* **2014**, *136*, 15781.
[44] D. N. Rockwood, R. C. Preda, T. Yücel, X. Q. Wang, M. L. Lovett, D. L. Kaplan, *Nat. Protoc.* **2011**, *6*, 1612.